A Numerical Study of Micro-heterogeneity Effects on Upscaled Properties of Two-phase Flow in Porous Media

D. B. DAS[1,*], S. M. HASSANIZADEH[2], B. E. ROTTER[3]
and B. ATAIE-ASHTIANI[4]
[1]*Department of Engineering Science, The University of Oxford, Oxford OX1 3PJ, U.K.*
[2]*Faculty of Civil Engineering and Geosciences, Delft University of Technology, P.O. Box 5048,
2600GA Delft, The Netherlands*
[3]*Department of Civil and Environmental Engineering, Edinburgh University, Edinburgh, Scotland,
U.K.*
[4]*Department of Civil Engineering, Sharif University of Technology, Tehran, Iran*

Abstract. Commonly, capillary pressure–saturation–relative permeability (P^c–S–K_r) relationships are obtained by means of laboratory experiments carried out on soil samples that are up to 10–12 cm long. In obtaining these relationships, it is implicitly assumed that the soil sample is homogeneous. However, it is well known that even at such scales, some micro-heterogeneities may exist. These heterogeneous regions will have distinct multiphase flow properties and will affect saturation and distribution of wetting and non-wetting phases within the soil sample. This, in turn, may affect the measured two-phase flow relationships. In the present work, numerical simulations have been carried out to investigate how the variations in nature, amount, and distribution of sub-sample scale heterogeneities affect P^c–S–K_r relationships for dense non-aqueous phase liquid (DNAPL) and water flow. Fourteen combinations of sand types and heterogeneous patterns have been defined. These include binary combinations of coarse sand imbedded in fine sand and vice versa. The domains size is chosen so that it represents typical laboratory samples used in the measurements of P^c–S–K_r curves. Upscaled drainage and imbibition P^c–S–K_r relationships for various heterogeneity patterns have been obtained and compared in order to determine the relative significance of the heterogeneity patterns. Our results show that for micro-heterogeneities of the type shown here, the upscaled P^c–S curve mainly follows the corresponding curve for the background sand. Only irreducible water saturation (in drainage) and residual DNAPL saturation (in imbibition) are affected by the presence and intensity of heterogeneities.

Key words: micro-heterogeneity, upscaling, capillary pressure–saturation–relative permeability relationships, DNAPL, water.

1. Introduction

Groundwater contamination by dense non-aqueous phase liquids (DNAPLs) is a serious environmental concern worldwide. Typical DNAPLs include, for

---

*Author for correspondence: Fax: +44-1865-283273; e-mail: diganta.das@eng.ox.ac.uk

example, tetracholoroethylene (PCE), polychlorinated biphenyl (PCB) oils, soltrol and creosote. They move as a separate phase in groundwater systems and can reach considerable depths below the water table because of their higher density than water. Properties of multiphase systems (e.g. interfacial tension, capillary pressure, density and viscosity of each fluid phase) and porous media (e.g. porosity, permeability, pore size distribution) are important in determining the extent and temporal aspects of their spreading behaviour in the subsurface. Moreover, heterogeneities in the media properties play a crucial role in this regard (Helmig, 1997; Miller *et al.*, 1998; de Neef, 2000). The transport processes are also governed by non-linear functional relationships between capillary pressure (P^c), saturation (S) and relative permeability (K_r).

In general, porous media heterogeneities have origins in various forms, for instance, presence of fractures, layers, lenses, etc. Most previous studies have focussed on implications of macroscopic and mega-scale heterogeneities and spatially varying permeability of porous media on saturated flow and transport (Yeh *et al.*, 1985; Mantaglou and Gelhar, 1987; Dekker and Abriola, 2000). Various aspects of multiphase flow in these heterogeneity patterns over different scales of observation have been studied by a large number of authors (e.g. Gray *et al.*, 1993; van Duijn *et al.*, 1995; Braun *et al.*, 1998; Oostrom *et al.*, 1999; van Kats, 1999; Dekker and Abriola, 2000; Zhou, 2001; Zhu, 2001; Ataie-Ashtiani *et al.*, 2001, 2002). These studies have clearly highlighted the significance of the variability in media and multiphase flow properties and the scales of observation on modelling the flow. However, effects of micro-heterogeneities of length scales of millimetres to tens of centimetres are often overlooked in these studies. Recent experimental and theoretical studies have shown that micro-heterogeneities have a significant effect on the spreading of organic liquids in the porous medium (see e.g. VEGAS experiments and, Ataie-Ashtiani *et al.*, 2001, 2002). Another issue of importance is that in laboratory measurements of capillary pressure–saturation–relative permeability curves (P^c–S–K_r) for two-phase flow in soil or rock samples, it is implicitly assumed that the sample is homogeneous. However, it is well known that even at that scale, some micro-heterogeneities may exist. These heterogeneous spots may have distinctly different multiphase flow properties than the surrounding media and affect the amount and distribution of both wetting and non-wetting fluid saturation significantly. This, in turn, may affect the measured two-phase flow relationships. Now, the question that arises is how these micro-heterogeneities affect measured P^c–S–K_r relationships. Based on numerical simulations, Ataie-Ashtiani *et al.* (2002) have shown that due to the presence of micro-heterogeneities, P^c–K_r–S relationships measured in the laboratory may be sensitive to the imposed boundary conditions. They have simulated a typical laboratory procedure for the simultaneous measurement of capillary pressure and relative permeability curves. The soil sample is simulated by a modelling domain of 10 cm × 10 cm. The soil is considered to be coarse sand embedded with blocks of finer sand. Boundary conditions are imposed such that colinear flow of two phases is established. Through

averaging the detailed simulation results, upscaled P^c–S–K_r relationships for the sample are obtained. Ataie-Ashtiani *et al.* (2002) have shown that the resulting P^c–S–K_r relationships are non-unique. Due to the presence of micro-heterogeneities in the medium; different boundary conditions result in different P^c–S–K_r relationships. Both drainage and imbibition curves have been studied. They have also investigated the directional dependence of constitutive relationships. However, a number of important issues remained unresolved. Among others, the implications of having different combinations of heterogeneities (e.g., having blocks of coarser sand in fine sand media) or variations in the amount of micro-heterogeneities (intensity of heterogeneity pattern) for the shape of effective P^c–S–K_r curves and residual fluid saturations were not investigated. Although two different patterns of a binary porous medium (staggered and non-staggered) were simulated, the amount of heterogeneous material in the samples was assumed to be the same in all cases. Therefore, one cannot draw any general conclusions as to whether the most important factor on determining the shape of laboratory scale P^c–S–K_r curves is the amount of imbedded micro-heterogeneities or the patterns.

This work aims at investigating how the variations in the nature, amount and distribution of sub-sample scale heterogeneities (micro-heterogeneities) affect P^c–K_r–S relationships for dense non-aqueous phase liquid (DNAPL) and water flow. Both staggered and non-staggered arrangements of the sand blocks are considered. Also, both cases of blocks of fine sand imbedded in coarse sand and vice versa are explored. P^c–S–K_r curves for different sand samples are compared with those of a reference medium consisting of one type of sand. This provides a good indication of the effects of variations in strengths and patterns of heterogeneity on the two-phase flow domain.

Another fundamental issue of utmost importance that needs to be addressed in detail is the role of microscopic heterogeneities on the hysteresis of constitutive relationships between P^c, S and K_r. Hysteresis is found in many engineering problems such as plasticity, ferromagnetism, and multiphase flow theories. In the context of multiphase flow, hysteresis refers to the dependence of P^c–S–K_r relationships on the fluid saturation history. It is attributed to two main factors: irreversibility of pore filling sequences and fluid entrapment (Collins, 1961; Bear, 1972; Dixit *et al.*, 1998). It is also often suggested that the hysteresis in K_r–S relationships is negligible in homogeneous porous media (Collins, 1961). This may be questionable in case of porous media with micro-heterogeneities. Previous studies on the hysteresis of P^c–S and K_r–S relationships have mostly focussed on homogeneous (isotropic or anisotropic) porous domains (Bear, 1972; Luckner and Schestakow, 1991; Beliaev and Hassanizadeh, 2001; van Kats and van Duijn, 2001) and rarely on heterogeneous media. Since micro-heterogeneities in the porous medium have considerable affects on the amount and distribution of both wetting and non-wetting fluids saturation (Ataie-Ashtiani *et al.*, 2001, 2002), it is reasonable to expect that capillary pressure and relative permeability will be subjected to stronger hysteresis in these media. In the present work,

numerical simulation techniques are employed which enable determination of the hysteretic behaviour of two-phase flow in heterogeneous porous media without having to resort to any simplifying assumptions. It is investigated whether various micro-heterogeneity patterns contribute to different hysteretic two-phase flow behaviours and to different fluid saturations at the end of drainage and imbibition. All simulations in this work are done in two-dimensional (2D). This is because we believe 2D simulations can provide good indications of various effects of micro-heterogeneity on P^c–S–K_r relationships without excessive computational cost.

2. Governing Equations and Description of Simulator

Mathematical modelling of the two-phase flow involves simultaneous solution of the equations for the conservation of mass and momentum supplemented by appropriate formulae for P^c–S–K_r relationships. As usually done, the Darcy's equation is used as the governing equation of motion for DNAPL and water:

$$\mathbf{q}_\gamma + \frac{K_{r\gamma}\mathbf{k}}{\mu_\gamma} \cdot (\nabla P_\gamma + \rho_\gamma g \hat{e}_g) = 0 \quad \text{for } \gamma \equiv \text{w, nw} \tag{1}$$

In the above equation, subscripts 'w' and 'nw' indicate the wetting (water) and non-wetting (DNAPL) phases, respectively. Furthermore, $\mathbf{q}$ is fluid flow velocity [LT^{-1}], K_r is relative permeability [–], $\mathbf{k}$ is intrinsic permeability tensor [L^2], μ is viscosity [$ML^{-1}T^{-1}$], P is pressure [$ML^{-1}T^{-2}$], ρ is density [ML^{-3}], g is gravity acceleration [LT^{-2}] and $\hat{e}_g$ is the unit vector in the positive vertical direction.

The conservation of mass in the two-phase system is described by the following equation:

$$\frac{\partial}{\partial t}(\phi \rho_\gamma S_\gamma) + \nabla \cdot (\rho_\gamma \mathbf{q}_\gamma) = 0 \quad \text{for } \gamma \equiv \text{w, nw} \tag{2}$$

where ϕ is porosity of the medium [–] and S is saturation [–].

The capillary pressure–saturation relationship is assumed to be given by the well-known Brooks–Corey formulae for non-deformable porous media (Brooks and Corey, 1964),

$$S_{ew} = \left(\frac{P^c}{P_d}\right)^{-\lambda} \quad \text{for } P^c \geqslant P_d \tag{3}$$

$$S_{ew} = 1 \quad \text{for } P^c \leqslant P_d \tag{4}$$

$$S_{ew} = \left(\frac{S_w - S_{rw}}{1 - S_{rw}}\right), \quad 0 \leqslant S_{ew} \leqslant 1 \tag{5}$$

where S_{ew} is effective saturation of the wetting phase, P_d is entry pressure for the non-wetting phase [$ML^{-1}T^{-2}$], λ is a pore size distribution index and S_{rw} is

irreducible wetting phase saturation. Although there are a number of other candidate models for describing the P^c–S dependence (Chen *et al.*, 1999), Brooks and Corey formulae are used in this work due to their empirical assumption of linear relationship between $\log(S_{ew})$ and $\log(P^c/P_d)$ with $-\lambda$ yielding the slope of the straight line. This enables the average pore size distribution index of a heterogeneous porous medium to be determined with the least computational effort.

In order to calculate the relative permeabilities of the heterogeneous sand samples, K_{rw} and K_{rnw}, the following empirical Brooks–Corey–Burdine formulae (Brooks and Corey, 1964) are adopted,

$$K_{rw} = S_{ew}^{(2+3\lambda)/\lambda} \tag{6}$$

$$K_{rnw} = (1 - S_{ew})^2 (1 - S_{ew}^{(2+\lambda)/\lambda}) \tag{7}$$

The relative permeability of a sand sample to a specific fluid phase can also be determined from the simulated results using the following formula:

$$K_{r\gamma} = \frac{q_\gamma \mu_\gamma L}{k \Delta P} \quad \text{for } \gamma \equiv w, nw \tag{8}$$

where L is the length of the sand sample across which the pressure gradient ΔP is imposed and q_γ is the flux through the sample.

The two-phase flow calculations in the present work have been carried out using the simulator STOMP (Lenhard *et al.*, 1995; White *et al.*, 1995; Oostrom *et al.*, 1997; Oostrom and Lenhard, 1998). STOMP has been developed as a general computational tool for simulating 11 different modes of multiphase flow in heterogeneous porous media. The code has been successfully validated and applied to simulate a variety of multiphase flow problems (e.g. Schroth *et al.*, 1998; White and Oostrom, 1998; Oostrom *et al.*, 1999; Ataie-Ashtiani *et al.*, 2001, 2002). The oil–water mode, which can utilise the governing equations described in the previous section, is employed in this work.

A note on the spatial discretisation of the governing model equations, as used in STOMP, must also be included here. This is done based on the standard finite volume method, FVM (Patankar, 1980; Versteeg and Malalasekera, 1995). One of the main advantages of the FVM is that it uses the cell-based integral method for discretising the model equations. This ensures that mass is globally conserved in the whole domain. Therefore, while dealing with heterogeneous porous domains, the simulation of discontinuous flow variables at block interfaces is more accurate than other numerical techniques such as the finite difference or finite element methods. The system of algebraic equations derived through the FVM discretisation of the governing conservation equations and other constitutive equations for P^c–S–K_r relations involve non-linear terms. These non-linear equations are reduced to linear forms by the application of the well-known Newton–Raphson iterative method for multiple variables. The temporal discretisation is based on the well-known implicit time stepping method. The implicit method is known for its ability to generate

stable numerical results, a fact also demonstrated by the oscillation free results obtained in this study (as shown later).

Finally, a key point that may be of interest to many readers, that is, the type of averaging techniques used to calculate the flow properties at the heterogeneity boundaries, should be mentioned. While upwind interfacial averaging is used for non-aqueous and aqueous relative permeabilities, for all other parameters harmonic interfacial averages are applied.

3. Description of Soil Heterogeneity Patterns and Numerical Simulations

In this section, we briefly describe the computational domains that represent various heterogeneous soil samples, the boundary conditions that are used, and the simulation procedure. Simulations are carried out over 2D square domains of 12 cm × 12 cm. This domain size is characteristic of the size of typical laboratory samples and, as shown by Ataie-Ashtiani *et al.* (2001), it is the size of the representative elementary volume (REV) for a medium with a periodic structure containing these heterogeneities.

The medium is composed of two different sand types, denoted by CS for coarse sand and FS for fine sand. Properties of the two sand samples and the fluids have been presented in Table I. Sand properties correspond to typical values found in the literature. For the fluid phase, as a common DNAPL contaminant of the subsurface, tetracholoroethylene (PCE) has been selected. The fluid properties are therefore based on real data. Of course there are numerous other organic liquid contaminants, which may be incorporated in the simulation. However, this is not considered to be of interest here as the effects of fluid properties on P^c–S–K_r relationships are well-documented (see e.g. Ringrose *et al.*, 1996).

Various heterogeneity patterns are considered. In total, 14 different combinations (C1–C14) of sand types and heterogeneity patterns are defined. As shown in Figure 1, the heterogeneity patterns are rectangular in shape and have a periodic structure. Patterns C1 and C2, which are not shown, correspond to reference

Table I. Sand and fluid properties used in simulation

Property	Units	Coarse sand (CS)	Fine sand (FS)	Water	DNAPL (PCE)
Permeability, k	m^2	5×10^{-9}	5×10^{-12}	–	–
Porosity, ϕ	–	0.40	0.40	–	–
Displacement pressure, P_d	N	370	1325	–	–
Pore size distribution index	–	3.86	2.49	–	–
Irreversible water saturation	–	0.078	0.098	–	–
Density	$kg\,m^{-3}$	2630	2650	1000	1630
Viscosity	$kg\,m^{-1}\,s^{-1}$			1×10^{-3}	0.9×10^{-3}

Figure 1. Sand samples with different heterogeneity patterns. Patterns C1 and C2, which are not shown in the figure, correspond to the reference samples consisting of homogeneous coarse (CS) and fine (FS) sand, respectively.

samples consisting of only coarse (CS) and fine (FS) sand, respectively. The heterogeneous blocks in Figure 1 (C3–C14) have two different values for the ratio of the area of the imbedded micro-heterogeneities to the total area of the domain, that is, 0.25 and 0.18. This ratio is a measure of the intensity or strength of the micro-heterogeneity. Blocks C3–C6 have a heterogeneity ratio of 0.25 and blocks C7–C14 have the ratio 0.18. Patterns similar to C4 and C6, where blocks of fine sand are imbedded in a coarse medium, have been studied by a number of authors (Durlofsky, 1991; Ataie-Ashtiani *et al.*, 2001, 2002). However, the studies on the flow behaviour when coarse sand blocks are present in a fine sand medium (e.g. C3 and C5) are not common. If flow of DNAPL and water takes place in the former case (finer heterogeneity), DNAPL may accumulate on top of the finer grained sand blocks and spread horizontally. In the latter case (coarser heterogeneity), entrapment of DNAPL may occur in the sand blocks with higher permeability. This may contribute to a significant rise of DNAPL concentration levels in the medium. Therefore, both combinations of sand types have significant practical relevance in determining two-phase flow behaviour in heterogeneous porous media. Hence, we have considered both binary samples in the analyses of DNAPL spreading behaviour and effects of heterogeneities on the P^c–S–K_r relationships. We have also chosen patterns where the top and bottom sand blocks are different in size (e.g. C9 and C11). The implications of the varying intensity of heterogeneity on the flow behaviour are investigated through these combinations. Both drainage and imbibition P^c–S–K_r relationships are studied.

Simulations carried out here are analogous to flow-through experiments in laboratories for measurements of P^c–S–K_r curves. The boundary conditions are defined such that the two fluid phases enter through the top face of the domain. The sidewalls are defined to be impermeable. The bottom face represents the exit boundary. In all simulations, a pressure difference (ΔP) of 1000 Pa across the domain is imposed for both wetting and non-wetting phases. The capillary pressure (P^{nw}–P^w) is chosen to be the same at both top and bottom ends. The imposed capillary pressure is varied by changing P^{nw} as described in detail below.

Drainage P^c–S–K_r curves for various heterogeneity patterns are obtained first. For this purpose, the whole domain is assumed to be fully saturated with water initially. A pressure difference of 1000 Pa across the sample for both phases is imposed. Obviously the water phase will flow. But the non-wetting phase will not flow as long as the imposed capillary pressure (P^{nw}–P^w) is less than the displacement pressure, P_d, of the background sand. Thus, first, the capillary pressure is set to a value slightly larger than P_d. As a result, a colinear flow of NAPL and water is established. The simulation is carried out until steady-state flow conditions are reached, that is, saturation at all grid points does not vary any more. The average saturation of the sand sample at steady state and the imposed P^c provide one point of the P^c–S graph. Also, from Equation (8), the relative permeability of the sand sample at this saturation can be determined, which yields one point of the K_r–S graph. Next, the imposed capillary pressure is increased incrementally and the simulation is continued until a new steady state is reached. A second point for P^c–S and K_r–S graphs is thus obtained. This procedure is repeated until a P^c of 10 000 Pa is reached. At this capillary pressure, the water saturation reaches its lowest value. This final wetting phase saturation at the end of drainage is defined as the irreducible water saturation (S_{rw}) in the medium.

To determine the imbibition P^c–S–K_r curves for different heterogeneity patterns, the reverse procedure is applied. However, in this instance, the starting point is the situation at the end of the drainage cycle; the sample is at irreducible water saturation and the capillary pressure is at 10 000 Pa. The capillary pressure is decreased incrementally from 10 000 Pa till it reaches a null value. This is done by keeping a constant wetting phase pressure but by decrementing the non-aqueous phase pressure. Similar to the drainage curves, each time the flow is allowed to reach steady state before the capillary pressure is decreased to a smaller value.

It must be noted that all simulations are done on a 2D horizontal plane so that gravity may be neglected. Any deviations observed in P^c–S–K_r curves, therefore, can be safely attributed to the presence of heterogeneity in the medium.

The numerical grid used in the simulation is a uniform mesh consisting of 48×48 square cells of size 2.5 mm $\times$ 2.5 mm. In order to check the numerical accuracy of results, the grid size is reduced by 4-fold. The refined mesh chosen for the test involves 96×96 square cells of size 1.25 mm $\times$ 1.25 mm. The results show negligible difference between P^c–S_w curves from the normal and refined meshes. A maximum difference of 1.4% in saturation is found at a given P^c between the

two P^c–S_w curves. The test shows that the numerical results presented in this paper are, in general, devoid of the grid size effects. For temporal discretisation, a time step of 1.0 s is employed for all simulations.

4. Results and Discussions

The main emphasis in this paper is to analyse various effects of micro-heterogeneities on the constitutive relationships between P^c, S and K_r for two-phase flow of DNAPL and water in porous media. In addition to properties, configurations, shape and size of micro-heterogeneities, other factors such as capillary pressure at the boundaries and pressure gradients across the domain influence the two-phase flow behaviour. However, detailed investigation for all and every aspect of the flow is not a practical option for a single paper even though it is likely that each factor affects the flow behaviour in different manner. If not mentioned otherwise, simulated results are discussed here for the porous media properties presented in Table I and boundary conditions discussed in the previous section. Although results presented in this paper correspond to laboratory scale samples we believe that these results are general enough that they can be extended to processes at larger scales such as those at field scale.

4.1. EFFECTS OF MICRO-HETEROGENEITY ON FLUID DISTRIBUTION

As mentioned before, the distribution of fluid saturation and the shape of P^c–S–K_r curves are influenced by a number of factors, which include intrinsic permeability (mostly for transient processes), pore size distribution and entry pressure of the media. In this section, effects of intensity and patterns of micro-heterogeneities on the two-phase flow behaviour are to be examined. This is done on the basis of DNAPL saturation plots and drainage upscaled P^c–S–K_r curves for different patterns.

Figure 2(a)–(n) presents plots of DNAPL saturation contours in blocks C1–C14 at a boundary capillary pressure of 10 000 Pa and a pressure gradient of 1000 Pa for each fluid phase. The saturation plots in homogeneous coarse (C1) and fine (C2) sand blocks are shown in Figure 2(a) and (b). The plots for blocks containing coarser heterogeneity, that is, coarse sand imbedded in fine sand medium (C3, C5, etc.) are shown in Figure 2(c)–(h). Figure 2(i)–(n) presents the contour plots for blocks containing finer heterogeneity, that is, fine sand imbedded in coarse sand. Differences in the saturation levels and pooling of DNAPL due to the presence of heterogeneities are clearly visible in these figures. The sharp contrast in the values of DNAPL saturation across the fine/coarse sand interface is due to a large contrast in the permeability of the two sands, which is chosen to be of the order of 10^3 (see Table I). It is also observed that the variation in the values of DNAPL saturation is larger if fine sand is imbedded in a coarse background material. In general, two trends in the saturation distributions are found depending on the combination of
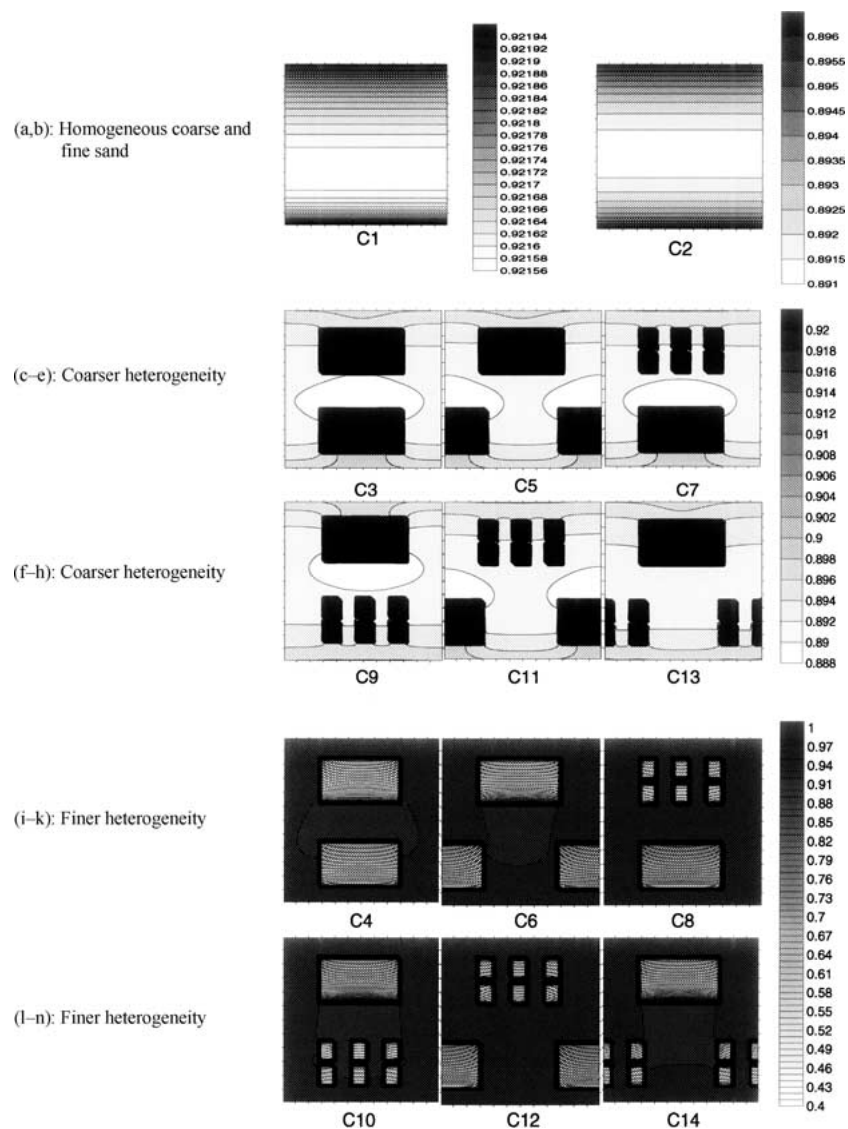
Figure 2. PCE saturation distributions for drainage in different heterogeneous blocks at capillary pressure of 10 000 Pa and pressure gradient of 1000 Pa. Effects of micro-heterogeneity on distribution of PCE are clearly observed.

binary sand types. When micro-heterogeneous blocks of coarse sand are present in fine sand medium (e.g. C3 and C5), DNAPL is accumulated inside the coarse sand blocks, which make them the zones of the highest DNAPL saturation. On the other hand, when fine sand blocks are present in a coarse medium (e.g. C4) the opposite phenomenon takes place. It is seen that DNAPL does not fully infiltrate the fine sand blocks even at high capillary pressure boundary conditions and they remain

at lower values of DNAPL saturation. The explanation of this different infiltration behaviour is sought later with respect to P^c–S–K_r relationships for various binary sand types.

4.2. FINER HETEROGENEITY PATTERNS AGAINST COARSER HETEROGENEITY PATTERNS

Simulated P^c–S–K_r curves for different intensities and patterns of micro-heterogeneous blocks (C3–C14) are presented in Figures 3(a)–(b) and 4(a)–(b). Figure 3(a) shows the P^c–S relationship when micro-heterogeneous blocks of fine sand are imbedded in coarse medium (e.g. C4). The corresponding K_r–S curves are given in Figure 3(b). Similarly, the P^c–S–K_r curves for the cases when micro-heterogeneous blocks of coarse sand are present in fine medium (e.g. C3) are shown in Figure 4(a) and (b). In these figures the curves for homogeneous sand media, that is, C1 and C2, are also given. It is evident that the upscaled curves for heterogeneous samples are distinctly different from either of the homogeneous samples. Also, the curves for finer heterogeneity samples are different from the curves for coarser heterogeneity samples. But for a given binary sample the intensity and the patterns of the heterogeneity do not have a very large effect on the shape of P^c–S–K_r curves.

In Figure 3(a) (for finer heterogeneity), it is evident that at higher values of water saturation (>0.48 in this case) the P^c–S curves lie close to the curve for coarse medium. This implies that the shape of the P^c–S curves are mostly determined by the entry pressure and pore size distribution for the coarse medium (surrounding medium) when the wetting phase saturation is high, or when capillary pressure is low. However, as wetting phase saturation decreases, or capillary pressure increases, the P^c–S curves start to deviate. The irreducible wetting phase saturation for the heterogeneous blocks is clearly larger than the values for both coarse and fine sand. This is in contrast to the common belief that they may lie in between the P^c–S curves for the homogenised sand. Such phenomenon is caused by the entrapment of water in the imbedded fine sand blocks in coarse medium, which results in a high average irreducible water saturation. As evident from the simulated curves for homogeneous coarse and fine sand media in Figure 3(a), there is a large difference in the values of entry pressure for these two sands (almost four times). By the time the capillary pressure at the boundary reaches the entry pressure for fine sand (i.e. 1325 Pa), the wetting phase saturation in the surrounding coarse medium is almost as low as its irreducible water saturation. Therefore, the relative permeability of the background coarse medium is almost zero when the boundary capillary pressure reaches the entry pressure for fine sand. Although at high capillary pressure water does exit from the fine sand blocks and DNAPL infiltrates from the coarse to finer grained media, amount of entrapped water in the fine sand remains high. This is illustrated clearly in DNAPL saturation plots for C4, C6, C8, etc. As a result of high amount of entrapped water in fine sand blocks, the average irreducible water
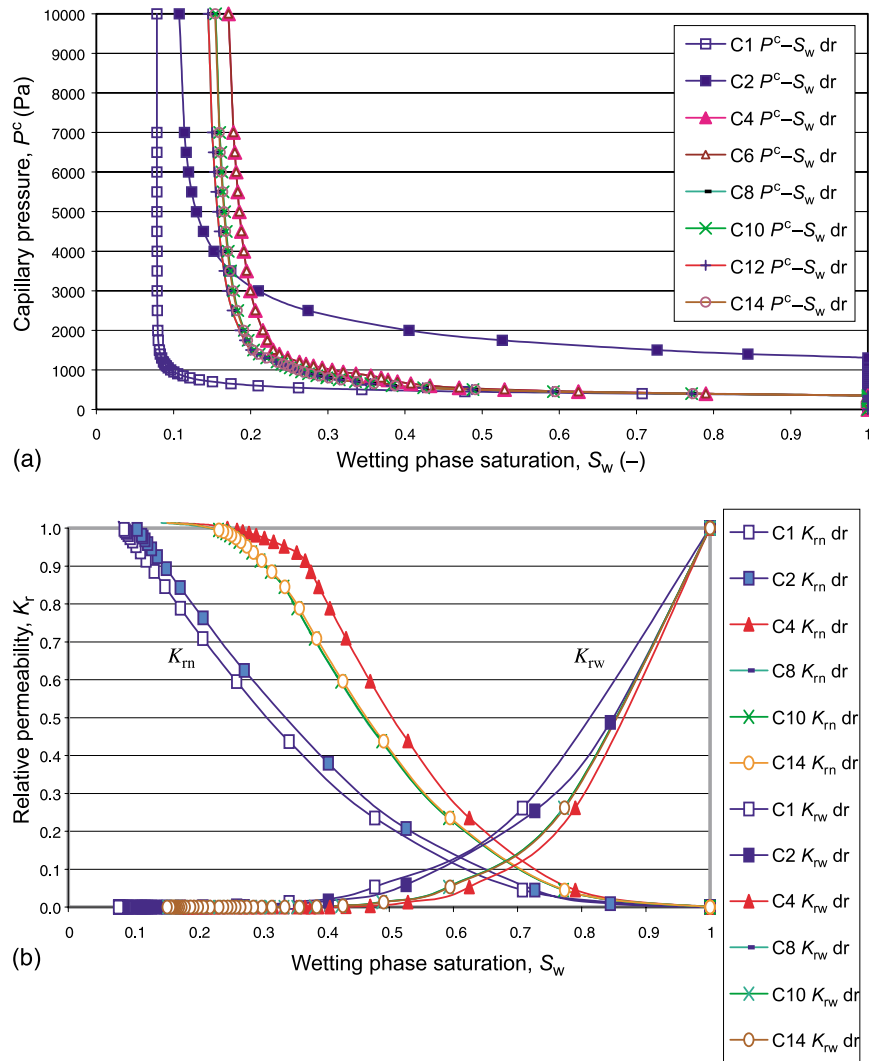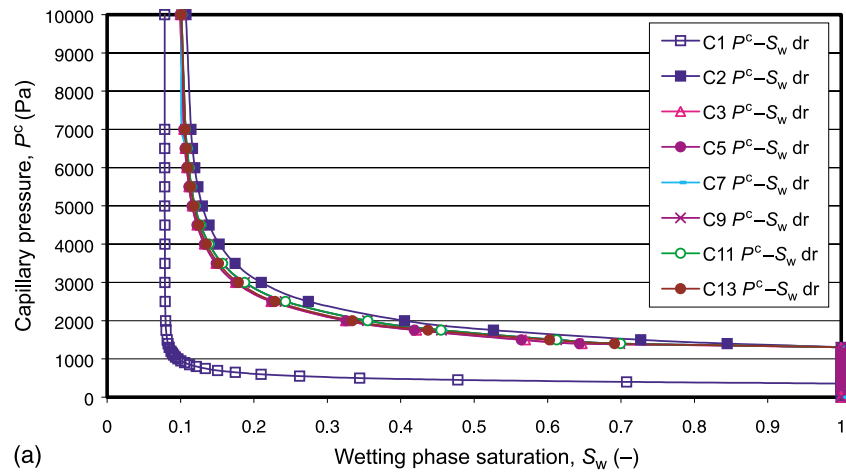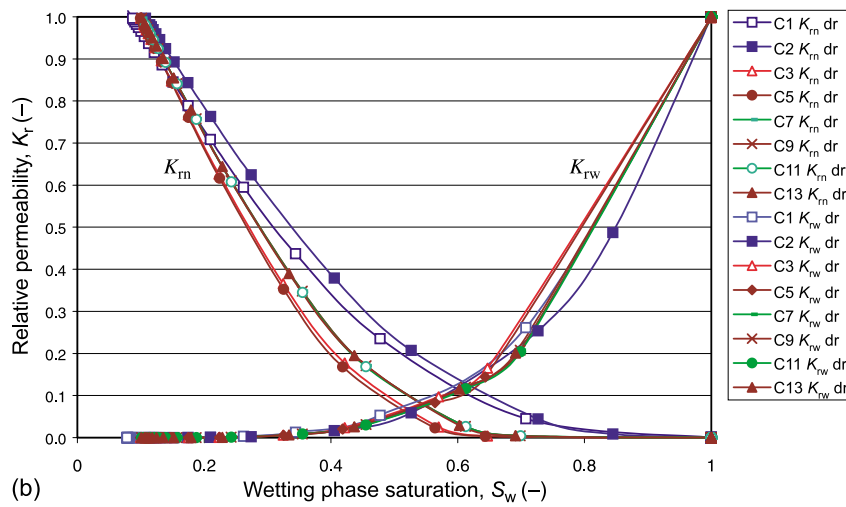
Figure 3. (a) Effects of finer heterogeneity on upscaled drainage capillary pressure–saturation (P^c–S) relationships in various heterogeneity patters. (b) Effects of finer heterogeneity on up-scaled drainage relative permeability–saturation (K_r–S) relationships in various heterogeneity patters.

saturation over the whole domain becomes higher than those for independent fine and coarse sand media (see Figure 3(a)).

Although at first sight the P^c–S relationship show negligible dependence on the intensity and pattern of these heterogeneity blocks, a close examination of the curves reveals more interesting facts. For example, the curves indicate that with higher intensity of the heterogeneity (higher amounts of fine sand) in the domain the irreducible wetting phase saturation is higher. Similarly, with increasing

Figure 4. (a) Effects of coarser heterogeneity on upscaled drainage capillary pressure–saturation (P^c–S) relationships in various heterogeneity patters. (b) Effects of coarser heterogeneity on upscaled drainage relative permeability–saturation (K_r–S) relationships in various heterogeneity patters.

resistance to flow of DNAPL by micro-heterogeneities (difficulty of flow because of the presence of fine sand), the irreducible saturation is higher. Evidence of these facts can be found if the P^c–S curves for the patterns, C4, C6, C8, C10 and C14 are examined. The amounts of fine sand in C4 and C6 blocks are the same and more than the other patterns (intensity of heterogeneity is higher). Hence, the irreducible wetting phase saturation in these blocks is almost the same and higher than those of other patterns. The amounts of fine sand in blocks C8, C10, C12 and C14 are the same but the resistance to DNAPL infiltration at the inlet (top) of the domain is least for C8 and C12 blocks. Therefore, the irreducible water phase saturation of these

two patterns is smaller than other heterogeneous blocks since in this case the water phase can be drained easier. The P^c–S curves for the patterns C10 and C14, which have the same amounts of fine sand, seem to match very well despite the fact that they have different arrangements of the blocks. Similar observation can be made for the case of P^c–S relationships for C4 and C6 blocks, which match well. This implies that the arrangements of the heterogeneities have negligible affect on the shape of P^c–S curves. But the intensity of micro-heterogeneity or the amounts of fine sand in coarse media may affect the shape of P^c–S relationships for two-phase flow in porous media. The corresponding drainage curves for the K_r–S relationships for these heterogeneity patterns (Figure 3(b)) further confirm that the intensity of heterogeneities in porous media may influence the constitutive relationships. For example, drainage K_r–S curves for C4 pattern, which has the highest intensity of heterogeneity, is distinctly different from the curves for homogeneous sand blocks and other heterogeneous patterns.

As evident in Figure 4(a) and (b), where coarse sand blocks are present in fine sand (C3, C5, C7, etc.) the effects of heterogeneities on the shape of drainage P^c–S–K_r curves and factors such as irreducible water saturation are less prominent. The P^c–S–K_r curves for these patterns lie between the curves for homogeneous coarse (C1) and fine media (C2) but very close to that for fine sand, that is, the background medium. In other words, lower average water saturation, or higher average DNAPL saturation, can be observed in these heterogeneous blocks than that of the pure background medium (fine sand) at a given capillary pressure. The reason is that once DNAPL enters the coarse sand, because of capillary forces, it tends to remain there. Moreover, at a given capillary pressure, the water saturation in coarse sand is lower than in fine sand. Thus the average saturation of the sample will be smaller than the case of homogeneous fine sand.

4.3. P^c–S CURVES IN DIFFERENT DIRECTIONS

Capillary pressure–saturation is a scalar property and, thus, it is not expected to be different in different directions. Nevertheless, it is not obvious that the upscaling procedures we have used here will yield the same P^c–S curves in different directions. In fact, vertical infiltration of NAPL is going to yield a different distribution of fluids than the horizontal infiltration. Thus, average P^c–S curves for the heterogeneous blocks for different flow directions have been compared to determine directional dependence, if any, on the constitutive relationships for the two-phase flow. For this purpose, drainage in both vertical and horizontal directions has been simulated for the same boundary capillary pressure and pressure gradient. The simulation procedure for horizontal flow is exactly the same as discussed before for vertical flow. However, in this case, the flow is defined to take place from left to right (see Figure 1) while upper and lower boundaries are assumed to be impermeable. As mentioned before, gravity is set to zero so that any deviation observed can be attributed to the heterogeneity. Typical results have been presented
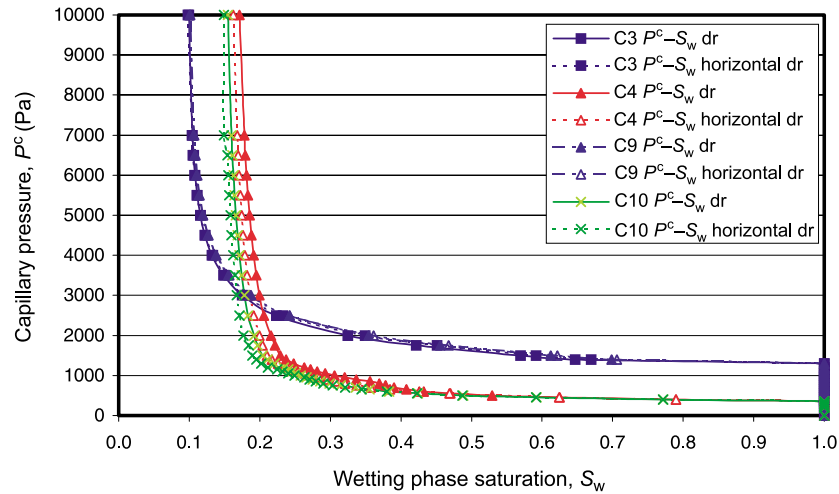
Figure 5. Effects of different flow directions on upscaled drainage capillary pressure–saturation (P^c–S) relationships in various heterogeneity patters. Unless otherwise mentioned, the curves are prepared for vertical flow of fluids.

in Figure 5 for patterns C3, C4, C9 and C10. These patterns include both binary combinations of sand types and varying intensities of heterogeneities (e.g. the intensity ratio of 0.25 for C3 and 0.18 for C9) for the same binary combination. Furthermore, it must be noted that C3 and C4 patterns are symmetrical along both flow directions but patterns C9 and C10 are asymmetrical. The results indicate that there is little directional effect of the heterogeneity on the P^c–S_w curves. Although in the case of finer heterogeneity patterns, the P^c–S curves may vary, for most practical purposes these variations are insignificant.

4.4. EFFECTS OF CONTRAST IN INTRINSIC PERMEABILITY

Sample results to determine the effects of the contrast in intrinsic permeabilities of coarse and fine sand on P^c–S relationships have been presented in Figure 6. The simulations have been done in order to determine whether average P^c–S relationships for heterogeneous media are sensitive to the contrast in permeability, which typically determines the heterogeneities in a porous medium. The contrast in permeability values is often called the degree of heterogeneity (ω). For example, Panfilov (2000, p. 5) has defined it as the ratio of permeabilities of two components, which form the heterogeneous media. In the present context, ω is calculated as the ratio of the intrinsic permeabilities of coarse to fine sand. For all previous simulations the degree of heterogeneity was 10^3. However, for this test, simulations using a value of 10 and 10^5 for the degree of heterogeneity have been carried out and the results compared. All other media and fluid properties are assumed to be the same for both sand types. The P^c–S curves are presented for C3 and C4 patterns (Figure 6). The main observation of the test is that for both patterns the average
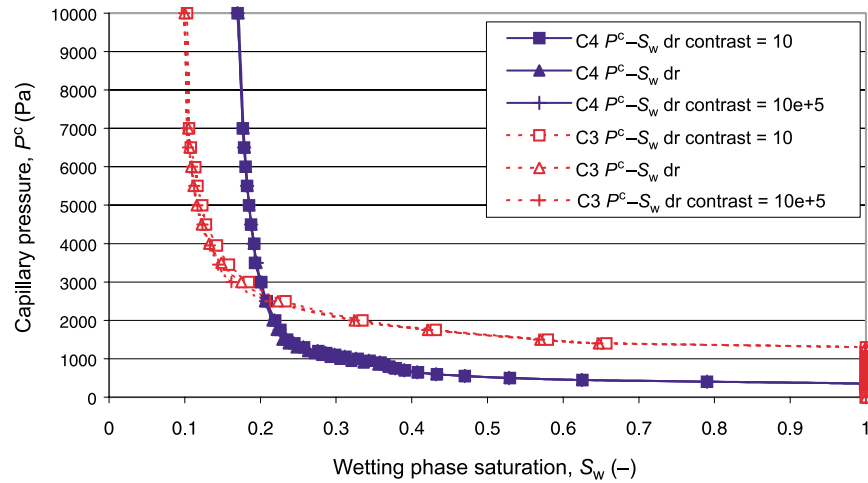
Figure 6. Effects of contrast in intrinsic permeability of coarse and fine sand on upscaled drainage capillary pressure–saturation (P^c–S) relationships. Unless otherwise mentioned, the curves are derived for a permeability contrast of $10e + 3$.

P^c–S curves are insensitive to the contrast in permeability. This confirms the fact that the P^c–S relationships in heterogeneous porous media are most sensitive to the properties of the individual sand types (e.g. pore size distribution index and entry pressure, etc.) and the dependence of these relationships on the contrast in intrinsic permeability of the sands can be neglected. Further, this is in contradiction to the common belief that average two-phase flow properties in heterogeneous media are affected by the permeability contrast (see, e.g. Ringrose *et al.*, 1996). However, our results should not have been unexpected, as the upscaled P^c–S curves have been based on steady-state saturation distributions, which will not be very sensitive to the contrast in intrinsic permeability.

4.5. EFFECTS OF DISTRIBUTION OF HETEROGENEITIES ON P^c–S CURVES

Other numerical simulations have been carried out in this work to determine whether the constitutive relationships depend on the distribution of heterogeneities. For this purpose, water drainage through two heterogeneous patterns has been considered, as shown in Figure 7(a). In the first instance, the heterogeneous medium contains one imbedded fine sand block at the centre of the medium (pattern HP1). Total area of this imbedded sand block is equal to the total area of the imbedded sand in patterns C3–C6, that is, $36 \, cm^2$ (same intensity of heterogeneity). In the second instance, the heterogeneous pattern (HP2) contains 30 randomly imbedded fine sand blocks of size $2 \, cm \times 0.5 \, cm$, yielding $30 \, cm^2$ of imbedded heterogeneities. Simulations have been carried out with the same boundary conditions. The P^c–S curves for these two heterogeneous patterns are then compared with those for homogeneous media (C1 and C2 blocks) and other typical finer heterogeneity
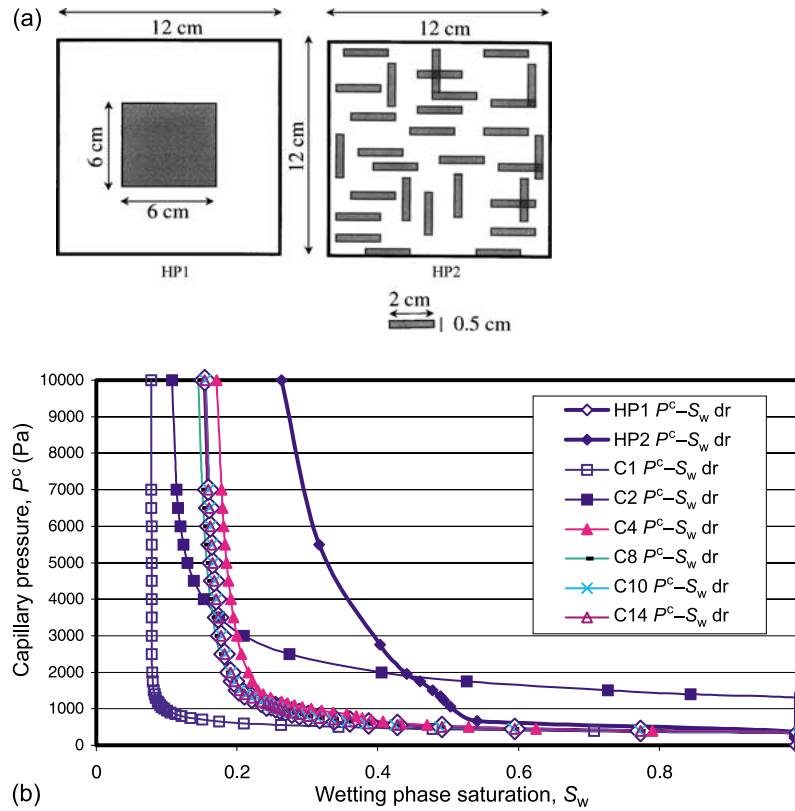
Figure 7. (a) Sample heterogeneity patterns (HP1 & HP2) to determine the effects of distribution of heterogeneity on upscaled drainage capillary pressure–saturation (P^c–S) relationships. (b) Effects of distribution of heterogeneity on upscaled drainage capillary pressure–saturation (P^c–S) relationships.

patterns. Results as presented in Figure 7(b) show that the P^c–S relationships might vary depending on the distribution of micro-heterogeneities. While the P^c–S curve for HP1 pattern is similar to those for other micro-heterogeneity patterns, the P^c–S curve for HP2 deviates from them. It seems to suggest that the distribution and the size of the micro-heterogeneity may also be important in determining the P^c–S relationships. However, this is a topic that can be explored further in a future work.

4.6. EFFECTS OF MICRO-HETEROGENEITIES ON IMBIBITION AND HYSTERESIS OF P^c–S–K_r RELATIONSHIPS

The main aim of this section is to discuss the effects of micro-heterogeneities on main imbibition curves and possible hysteresis in P^c–S–K_r relationships. As mentioned earlier, simulations for imbibition were carried out assuming the heterogeneous medium to be at irreducible water saturation. Furthermore, no hysteresis in P^c–S–K_r relationships for individual coarse or fine sand is assumed, that is, they

are the same for both drainage and imbibition relationships. Figure 8(a) and (b) shows the imbibition P^c–S curves for different heterogeneity patterns. In these figures, the upscaled drainage curves are also included so that hysteresis between the relationships, if any, can be ascertained. Figure 8(c) presents upscaled imbibition and drainage K_r–S curves for a number of heterogeneity patterns. In all cases
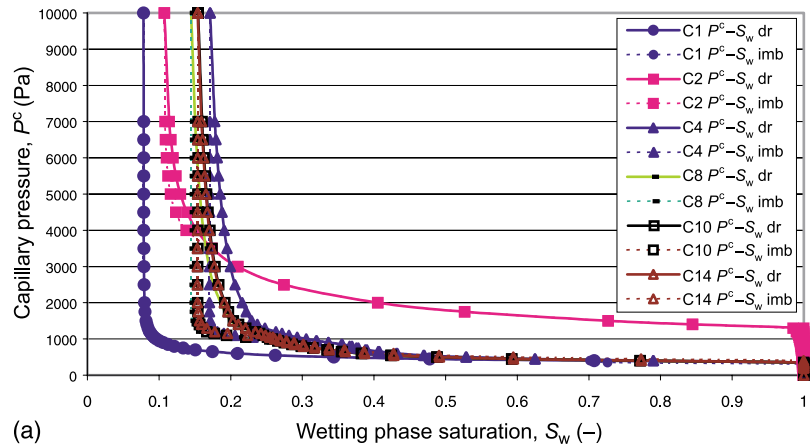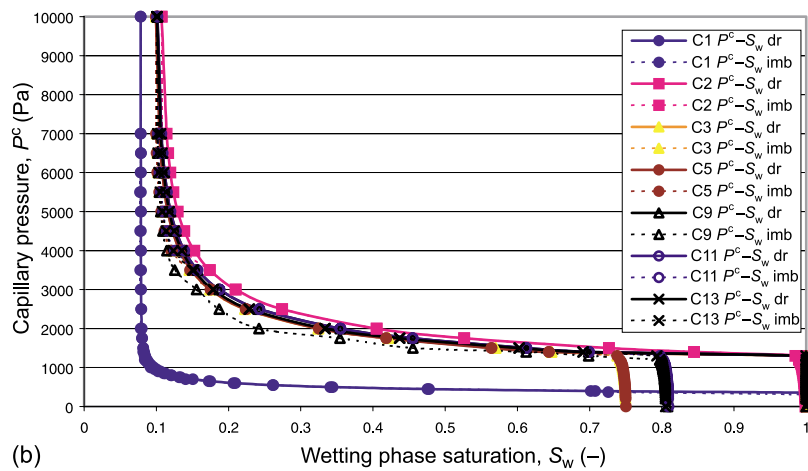
Figure 8. (a) Effects of microheterogeneity on upscaled imbibition capillary pressure–saturation (P^c–S) curves for finer heterogeneity patterns. The curves are also compared with drainage curves and the effects of various intensity of heterogeneity on irreducible and residual PCE saturations are determined. (b) Effects of microheterogeneity on upscaled imbibition capillary pressure–saturation (P^c–S) curves for finer heterogeneity patterns. The curves are compared with drainage curves and the effects of various intensity of heterogeneity on irreducible and residual PCE saturations are determined. (c) Effects of micro-heterogeneity on upscaled imbibition relative permeability–saturation (K_r–S) curves for various heterogeneity patterns. The curves are compared with drainage K_r–S curves and the effects of various intensity of heterogeneity on the hysteresis of K_r–S curves are determined.
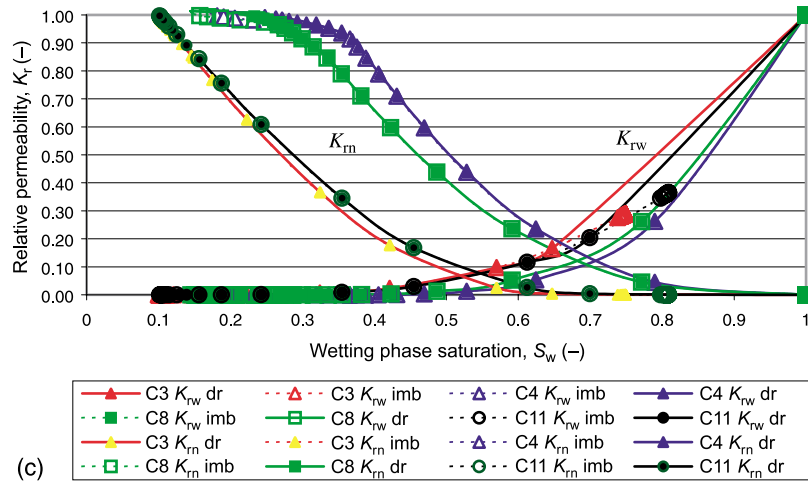
Figure 8. Continued.

the imbibition curve starts at $P^c = 10\,000$ Pa and at the irreducible water phase saturation reached at the end of the preceding drainage cycle.

Figure 8(a) presents imbibition and drainage P^c–S curves for finer heterogeneity patterns (e.g. C4, C8, etc.). For imbibition curves (dotted lines), it is observed that the capillary pressure has to decrease considerably (around 1500 Pa) before water invades the sample. This corresponds to what is normally observed in laboratory experiments. Thereafter, water saturation increases with continued lowering of capillary pressure and it reaches unity (i.e. no residual DNAPL saturation) when capillary pressure becomes equal to or smaller than the entry pressure of the coarse sand. This happens because, on one hand, there is no residual NAPL saturation in the P^c–S curves at the two reference sand media. On the other hand, once the background coarse medium is invaded by water, the fine sand heterogeneity blocks will also be saturated by water. As a result, there will be no trapped NAPL in these blocks. This is not, however, the case when coarse sand blocks are imbedded in fine sand (patterns C3, C5). For such heterogeneous samples, water may invade the background fine sand, by pass the coarse sand blocks and entrap the NAPL in those blocks. This results in residual NAPL saturation in the upscaled imbibition P^c–S curves as is evident in Figure 8(b) (dashed line). Note that none of the homogeneous sample, C1 or C2, shows a residual NAPL saturation. It is also obvious that the amount of residual NAPL is directly proportional to the intensity of heterogeneity; it is largest for samples C3 and C5. Further, inspection of graphs in Figure 8(a) and (b) show that there is some degree of hysteresis in P^c–S relationships. This is, however, not significant. Obviously, if hysteresis were included in P^c–S curves for the reference sand media, it would have directly resulted in the same degree of hysteresis in upscaled P^c–S curves.

The upscaled drainage and imbibition K_r–S curves for four typical heterogeneity patterns, namely, C3, C4, C8, C11, are compared in Figure 8(c). It appears that the

presence of micro-heterogeneity does not induce any hysteresis in K_r–S curves except that in the case of coarser heterogeneity patterns (e.g. C3 and C11), the wetting phase K_r-curve ends at a saturation value less than unity.

5. Conclusions

A systematic analysis of various effects of micro-heterogeneities on spreading behaviour of a DNAPL (PCE) in water-saturated sand samples has been presented. Average capillary pressure–saturation–relative permeability (P^c–S–K_r) relationships for two binary combinations of sand, that is, coarse sand blocks embedded in fine sand and vice versa, and various heterogeneity patterns have been obtained. Both drainage and imbibition relationships have been derived. In this work, capillary pressure specified at the boundary of the domains is used to plot the P^c–S–K_r curves. Although we have used a two-dimensional domain in our simulations, we believe that if a similar intensity of heterogeneity is used for 3D simulations, similar behaviours of upscaled P^c–S–K_r relationships will be observed.

Our results show that, for the given soil sample and boundary conditions, different P^c–S–K_r curves can be obtained depending on the intensity of heterogeneity. Obviously, local fluid saturation distributions are significantly affected; but their influence on average P^c–S–K_r relationships depends on the type of binary sand combinations.

When coarse sand blocks are present in fine sand, in drainage, the upscaled P^c–S–K_r curves are more or less the same as the corresponding curves for background fine sand. The same can be said about imbibition curves except that the residual DNAPL saturation is larger than for either of the two homogeneous sand blocks.

If fine sand is present in a coarse medium, the P^c–S–K_r relationships match very well with those for background coarse sand, particularly at high water saturation. The only difference is that the irreducible wetting phase saturation is larger than homogeneous coarse or fine sand. It has also been found that generally the irreducible water saturation and residual NAPL saturation are functions of the intensity of heterogeneity; the higher the intensity the larger the corresponding saturation value.

Most P^c–S–K_r curves presented here are for the flow direction top to bottom in blocks shown in Figure 1. We have investigated the directional dependence of these P^c–S curves and our results show that they do not depend on flow directions. Our simulations have also indicated that the upscaled P^c–S curves are not sensitive to the contrast in permeabilities of coarse and fine sand or to the form of heterogeneity patterns (staggered and non-staggered).

References

Ataie-Ashtiani, B., Hassanizadeh, S. M., Oostrom, M., Celia, M. and White, M. D.: 2001, Effective parameters for two-phase flow in a porous medium with periodic heterogeneities, *J. Contamin. Hydrol.* **49**, 87–109.

Ataie-Ashtiani, B., Hassanizadeh, S. M. and Celia, M.: 2002, Effects of heterogeneities on capillary pressure–saturation–relative permeability relationships, *J. Contamin. Hydrol.* **56**, 175–192.

Bear, J.: 1972, *Dynamics of Fluids in Porous Media*, American Elsevier Publishing Company Inc., New York.

Beliaev, A. Y. and Hassanizadeh, S. M.: 2001, A Theoretical model of hysteresis and dynamic effects in the capillary relation for two-phase flow in porous media, *Transport in Porous Media* **43**, 487–510.

Braun, C., Hassanizadeh, S. M. and Helmig, R.: 1998, Two-phase flow in stratified porous media: effective parameters and constitutive relationships. *Proceedings of the Computational Methods in Water Resources*, Crete, Greece, 15–19 June, pp. 43–50.

Brooks, R. H. and Corey, A. T.: 1964, *Hydraulic Properties of Porous Media. Hydrology Paper*, Vol. 3, Civil Engineering Department, Colorado State University, Fort Collins.

Chen, J., Hopmans, J. W. and Grismer, M. E.: 1999, Parameter estimation of two-fluid capillary pressure–saturation and permeability functions, *Adv. Water Res.* **22**, 479–493.

Collins, R. E.: 1961, *Flow of Fluids Through Porous Materials*, Reinhold, New York.

de Neef, M.: 2000, Modelling capillary effects in heterogeneous porous media, PhD Thesis, Delft University of Technology, Delft, The Netherlands.

Dekker, T. L. and Abriola, L. M.: 2000, The influence of field-scale heterogeneity on the infiltration and entrapment of dense non-aqueous phase liquids in saturated formations, *J. Contamin. Hydrol.* **42**, 187–218.

Dixit, A. B., McDougall, S. R. and Sorbie, K. S.: 1998, A pore level investigation of relative permeability hysteresis in water-wet systems, *SPE J.* **3**(2), 115.

Durlofsky, L. J.: 1991, Numerical calculation of equivalent grid block permeability tensor for heterogeneous porous media, *Water Res. Res.* **27**, 699–708.

Gray, W. G., Lijnse, A., Kolar, R. L. and Blain, C. A.: 1993, *Mathematical Tools for Changing Scales in Analysis of Physical Systems*, CRC Press, Inc., Boca Raton, FL.

Helmig, R.: 1997, *Multiphase Flow and Transport Processes in the Subsurface: A Contribution to the Modeling of Hydrosystems*, Springer-Verlag, Berlin.

Lenhard, R. J., Oostrom, M. and White, M. D.: 1995, Modelling fluid-flow and transport in variably saturated porous media with STOMP simulator. 2. Verification and validation exercises, *Adv. Water Res.* **18**(6), 365–373.

Luckner, L. and Schestakow, W.: 1991, *Migration Processes in the Soil and Groundwater Zone*, Lewis Publishers, Inc.

Mantaglou, A. and Gelhar, G. W.: 1987, Stochastic modelling of large-scale transient unsaturated flow system, *Water Res. Res.* **23**(1).

Miller, C. T., Christakos, G., Imhoff, P. T., McBride, J. F. and Pedit, J. A.: 1998, Multiphase flow and transport modelling in heterogeneous porous media: challenges and approaches, *Adv. Water Res.* **21**, 77–120.

Oostrom, M. and Lenhard, R. J.: 1998, Comparison of relative permeability–saturation–pressure parametric models for infiltration and redistribution of a light nonaqueous porous liquid in sandy porous media, *Adv. Water Res.* **21**, 145–157.

Oostrom, M., Hofstee, C. and Dane, J. H.: 1997, Light non-aqueous phase liquid movement in a variable saturated sand, *Soil Science Soc. Am. J.* **61**, 1547–1554.

Oostrom, M., Hofstee, C., Walker, R. C. and Dane, J. H.: 1999, Movement and remediation of trichloroethylene in a saturated heterogeneous porous medium. 1. Spill behavior and initial dissolution, *J. Contamin. Hydrol.* **37**(1–2), 159–178.

Panfilov, M.: 2000, Macroscale models of flow through highly heterogeneous porous media. *Theory and Applications of Transport in Porous Media*, Vol. 16, Kluwer Academic Publishers, Dordrecht, The Netherlands.

Patankar, S. V.: 1980, *Numerical Heat Transfer and Fluid Flow*, Hemisphere, Washington, DC.

Ringrose, P. S., Jensen, J. L. and Sorbie, K. S.: 1996, Use of geology in the interpretation of core-scale relative permeability data, *SPE Formation Eval.* 171–176.

Schroth, M. H., Istok, J. D., Selker, J. S., Oostrom, M. and White M. D.: 1998, Multifluid flow in bedded porous media: laboratory experiments and numerical simulations, *Adv. Water Res.* **22**(2), 169–183.

van Duijn, C. J., Molenaar, J. and de Neef, M. J., 1995: The effect of capillary forces on immiscible two-phase flow in heterogeneous porous media, *Transport in Porous Media* **21**, 71–93.

van Kats, F.: 1999, Aspects of upscaling in multi-phase flow problems, PhD Thesis, Delft University of Technology, The Netherlands.

van Kats, F. and van Duijn, C. J.: 2001, A mathematical model for hysteretic two-phase flow in porous media, *Transport in Porous Media* **43**(2), 239–263.

Versteeg, H. K. and Malalasekera, W.: 1995, *An Introduction to Computational Fluid Dynamics: the Finite Volume Method*, Addition Wesley Longman Ltd., Essex.

White, M. D. and Oostrom, M.: 1998, Modelling surfactant-enhanced nonaqueous-phase liquid remediation of porous media. *Soil Science* **163**(12), 931–940.

White, M. D. and Oostrom, M.: 2000, Technical Report, Pacific Northwest National Laboratory, Richland, Washington.

White, M. D., Oostrom, M. and Lenhard, R. J.: 1995, Modelling fluid-flow and transport in variably saturated porous media with STOMP simulator. 1. Nonvolatile 3-phase model description, *Adv. Water Res.* **18**(6), 353–364.

Yeh, T.-C., Gelhar, L. W. and Gutjahr, A. L.: 1985, Stochastic analysis of unsaturated flow in heterogeneous soils. 3. Observation and applications, *Water Res. Res.* **21**, 465–471.

Zhou, W.: 2001, Numerical simulation of two-phase flow in conceptualized fractures, *Environ. Geol.* **40**, 797–808.

Zhu, J.: 2001, Transport and fate of nonaqueous phase liquid (NAPL) in variably saturated porous media with evolving scales of heterogeneity, *Stochastic Environ. Res. Risk Assess.* **15**, 447–461.